ANL/PPRNT--89-144

2-D ACAR MEASUREMENTS OF Ni_3Al*

DE89 008338

L.C. Smedskjaer, A. DasGupta,** D.G. Legnini, and M.D. Stahulak

Materials Science Division

Argonne National Laboratory, Argonne, Illinois 60439

July 1987

jmg

DISCLAIMER

Submitted to Philosphical Magazine B.

*Research jointly supported U.S. Department of Energy, BES-Materials Sciences, under Contract #W-31-109-ENG-38 at Argonne National Laboratory and by the Office of Naval Research under Interagency Agreement 40-1515-84 in Navy N00014-85-F-0067 with Martin Marietta Energy Systems, Inc.

**Metals & Ceramics Division, ORNL, Oak Ridge, TN 37831.
Present address: USDOE, Chicago Operations Office, Argonne, IL 60439.

2-D ACAR MEASUREMENTS OF Ni_3Al*

L. C. Smedskjaer**, A. DasGupta†,††, D. G. Legnini**, and M. D. Stahulak**.

**Materials Science Division
Argonne National Laboratory, Argonne, Illinois 60439.
†Metals and Ceramics Division
Oak Ridge National Laboratory, Oak Ridge, Tennessee 37831

Abstract:

In connection with a detailed study of the electronic structure and stability of the aluminides $(Ni,Fe)_3Al$, 2-D ACAR positron annihilation measurements were made on a Ni_3Al single crystal to study the Fermi surface. The results for Ni_3Al have been compared with results for pure Ni. Strong similarities were found for the electronic structures of these materials. Theoretical calculations of the Fermi surface for Ni_3Al are in good agreement with the experimental results. The Γ_{16} sheet, not previously observed in any experiment, has now been observed for the first time in Ni_3Al.

---

* Research jointly sponsored by the Division of Materials Sciences, U. S. Department of Energy under Contract W-31-109-ENG-38 with Argonne National Laboratory and by the Office of Naval Research under Interagency Agreement 40-1515-84 in Navy N00014-85-F-0057 with Martin Marietta Energy Systems, Inc.

†† Present address: U.S. Department of Energy, Chicago Operations Office, Argonne, IL 60439.

Introduction:

In connection with a detailed study of the electronic structure and stability of the aluminides, $(Ni,Fe)_3Al$, 2D-ACAR positron-annihilation measurements were made on a Ni_3Al single crystal to study the Fermi surface. It is well known that Ni_3Al exhibits strong paramagnetism of itinerant electrons at room temperature. Bull et al. (1985) have pointed out that a theory (e.g. Moriya et al. (1979)) explaining the role played by the generalized spin-density fluctuation in itinerant-electron magnetism requires detailed information about the Fermi surface, the electronic band structure, and the density of states. Hence the interest in the Fermi surface of Ni_3Al is related to both the electronic stability and other magnetism-related physical properties of the material. Theoretical calculations of the Fermi surface in this material have been performed in the past by Fletcher (1971,1972) and by Buiting et al. (1983). Experimentally, the Fermi surface of Ni_3Al has been studied via de Haas-van Alphen (dHvA) measurements by Sigfusson et al. (1984). Although their measurements are in basic agreement with the theoretical calculations of Buiting et al. (1983) when modified, the dHvA measurements have not revealed some important details of the calculated Fermi surface. One such feature is the Γ_{16} sheet, the existence of which has been consistently predicted in all the theoretical calculations thus far, but has not been experimentally verified. The presence of the Γ_{16} sheet has also been predicted for Ni_3Ga (Kubo and Wakoh,1983,1987, Shiotani et al. 1986), although the 2D-ACAR measurements by Bull et al. (1985) and Shiotani et al. (1986) in Ni_3Ga were inconclusive in demonstrating its presence. In the present work, an account of the first 2D-ACAR measurements on a Ni_3Al single crystal is provided, detailing a quantitative comparison between the measured Fermi surface and theoretical

calculations. These results provide, for the first time, a clear verification of the Γ_{16} sheet in the Fermi surface.

Experimental:

For the purpose of the 2D-ACAR measurements, a $Ni_{76.5}Al_{23.5}$ single crystal, approximately 1 cm x 1 cm x 2 mm in size, was cut with a (110) face from a directionally solidified material obtained from United Technologies (Gell et al. 1980). This material, consisting of a single [100]-oriented γ' dendritic structure with traces of the γ phase present inside the dendrite arms (Fig. 1), was given a two-step homogenization annealing treatment, 100 h at 1100°C and 100 h at 1000°C, to dissolve the γ phase and obtain a homogeneous γ' single crystal. The single-phase and -crystal character of the sample were checked by optical microscopy, and x-ray diffractometry was used to determine the orientation as well as the mosaic spread (0.5°).

This crystal was mounted with the [110] direction toward the source and the [001] direction toward the Anger cameras, resulting in integration along the [001] direction. A total of 12×10^6 coincidence counts was collected and binned in a 256 by 256 matrix (0.17 mrad/channel). The instrumental resolution of 0.34 by 0.34 mrad should be corrected for thermal broadening to obtain the effective resolution of $\approx$ 0.6 by 0.6 mrad, since the measurements were made at room temperature. Following the experiment, the momentum-dependent efficiency matrix was determined experimentally and used to correct the data. The data were found to exhibit C_{4v} symmetry within experimental error. After C_{4v} symmetrization the LCW theorem (Lock et al. 1973) was used to fold the data back into the first Brillouin zone. This is called the k-space representation in the following, in contrast to the measured representation, p-space. Here, $k = p+nG$, where G is a reciprocal lattice vector, p the

measured momentum, while n is an integer such that $|k| < G/2$. Thus the k-space representation corresponds to the reduced zone scheme representation. In regard to the k-space representation, minor systematic errors may occur if, for example, the measured momentum $p' = p\cdot(1+\varepsilon)$ and/or the assumed reciprocal lattice vector $G' = G\cdot(1+\delta)$, where p is the true momentum and G is the true lattice vector. Then, $k' = p'+nG' = k+p\varepsilon+nG\delta \approx k+p\cdot(\varepsilon+\delta)$, and considering that momenta $p \approx 20$ mrad contribute significantly to the first zone, systematic errors of ≈ 0.2 mrad will occur if $(\varepsilon+\delta)\approx 1\%$. For this reason the positional errors in the first zone were estimated to be ≈ 0.2 mrad. In addition, channels containing the folding axis were considered to be statistically less reliable and have been omitted from our graphic representations. The results are shown in Figs. 2 and 3.

The Ni_3Al data will be compared with data for pure Ni (to be published). The Ni data were obtained and treated in the same fashion as the Ni_3Al data, except that a dispersion of 0.34 mrad/channel was used. In order to compare Ni and Ni_3Al, the ordered alloy Ni_3Ni having the $L1_2$ structure is introduced. Thus Ni_3Ni can be obtained from Ni_3Al by substituting Ni atoms for the Al atoms and adjusting the lattice parameter.

Discussion:

The following is largely based on the k-space representation of the 2-D ACAR data, which will now be considered .

For positrons having an equal probability of annihilation with all band electrons, the filled bands would not give rise to a k-dependence of the 2-D ACAR surface and the observed dependence would be entirely due to the partially filled bands. Rapid changes in the 2-D ACAR surface would then only be found at points where the integration direction is tangent to a Fermi surface. However, the

annihilation cross section depends on the electron- and positron-wave functions, causing annihilations to occur preferentially with some of the electrons, and the filled bands may, therefore, contribute to the observed k-dependence. This has been discussed in more detail in the original LCW work (Lock et al. 1973) as well as more recently (Berko 1983, Minjarends 1983).

The import of a k- or p-space dependence arising from effects other than the Fermi breaks, is that it may cause a minor displacement in the apparent location of the Fermi breaks for situations with finite experimental resolution. Such displacements can, of course, be reduced by an improvement in the resolution.

The k-space dependence is smaller than the corresponding p-space dependence, and thus, a k-space representation is sometimes more appropriate when analyzing the Fermi surface topology. It should be pointed out that the k-space representation contains no information about the Umklapp processes and detailed theoretical comparisons with data are therefore often done entirely in p-space.

The Ni_3Al measurements (Fig. 3) may be compared with the experimental results for Ni_3Ga (Bull et al. 1985, Shiotani et al. 1986). One observes that the results for Ni_3Ga appear smoother than the present results, while the theoretical calculations for Ni_3Ga (Shiotani et al. 1986) exhibit a considerable amount of structure. One also notes that the present results have characteristics similar to the theoretical results for Ni_3Ga, which might be anticipated since Ga and Al are electronically similar.

The present data will now be considered from the viewpoint of anisotropy.

The Fermi surface in Ni_3Al is anisotropic as shown in Fig. 4 (Buiting et al. 1983), consisting of four hole sheets Γ_{14} thru Γ_{17} and two small electron sheets R_{18} and R_{19}. In the present experiment, the Γ_{14}/Γ_{15} sheets cannot be resolved from one another, nor can the R_{18}/R_{19} sheets be resolved. Figure 4 shows that a

neck appears at the X point due to the Γ_{17} sheet and that both the Γ_{16} and Γ_{17} sheets have lobes in the [111] direction. One expects that an anisotropy study of the data could reveal some of these Fermi surface features.

In the case of Ni_3Ga, theoretical calculations predicted a strong and anisotropic k-dependence due to the filled bands (Bull et al. 1985, Shiotani et al. 1986, Kubo and Wakoh 1987). One anticipates a similar k-dependence in Ni_3Al. It will be shown that the slowly varying anisotropic dependence seen in Fig. 2 and Fig. 3 can be reduced by the subtraction of an isotropic p-dependence. It is emphasized that this is not an attempt to remove the influence of the filled bands entirely, but to reduce their appearence in the data.

The Ni_3Al data are anisotropic both in p- and k-space, and it will be shown that the topology of the Fermi surface contributes significantly to this anisotropy. Kubo and Wakoh (1987) concluded that the Fermi surface topology of Ni_3Ga did not contribute significantly to the anisotropy of the 1-D ACAR spectra. This is also the case for 1-D ACAR spectra for Ni_3Al, but not for 2-D ACAR spectra. In Fig. 5, the difference between the [110] and [100] directions is plotted for 1-D and 2-D ACAR spectra, respectively. The peaks seen in the 2-D ACAR spectrum originate from differences between the Fermi surface topology in the [110] and [100] directions. In contrast, the 1-D ACAR spectrum shows no similar effects . The results shown in Fig. 5 are expected, since the Brillouin zone in Ni_3Al is small, and within each zone multiple Fermi surfaces are found, resulting in the rapid variations seen in the anisotropic 2-D ACAR signal. However, integrating this 2-D ACAR surface in order to form the 1-D ACAR data will destroy much of the information about the topology as can be seen from Fig. 5.

In order to study the anisotropy, a method similar to that used by others (e.g. Berko et al. 1977) was followed by subtracting a radially symmetric surface

from the observed data in p-space. The isotropic surface is enveloped by the observed surface, while always as high as possible. Specifically, the value of the radially isotropic surface at radius p_r and angle p_θ is $N(p_r,p_\theta) \approx \mathrm{Min}\{ N(p_x,p_y) \}$, where $N(p_x,p_y)$ is the observed value at (p_x,p_y) while $\mathrm{Min}\{ N(p_x,p_y) \}$ is the smallest value observed for (p_x,p_y) fullfilling $p_r^2=p_x^2+p_y^2$. Afterwards, the isotropic surface was smoothed, eliminating sharp characteristics in this surface. Henceforth, anisotropy is taken to mean the remainder when this isotropic surface has been subtracted.

The results, in p-space, are illustrated in Fig. 6 showing the 2-D sections along [110] and [100] and the isotropic curves for Ni and Ni_3Al. The differences between three 2-D sections and the isotropic curves are also shown. The small negative values occurring in the difference curves are a consequence of the smoothing of the isotropic surface.

It is seen that the subtraction of the isotropic curves has reduced the slowly varying component of the p-space dependence considerably. In the [100] direction the anisotropic curves are almost entirely dominated by a rapidly varying signal, while some slowly varying p-space dependence is retained along the [110] direction. The anisotropic curves contain only a few percent of the annihilations, which is not surprising, considering the many filled bands in Ni_3Al and Ni. The subtracted isotropic curves contain slowly varying signals, including those from the partially filled bands. Therefore, the anisotropic curves do not simply represent the partially filled bands; they contain all rapidly varying signals, especially those originating from the Fermi breaks, as well as rapidly varying properties of the filled bands, if any. The purpose here has been to expose the Fermi breaks more clearly and independently of a slowly varying background.

For $p > 6$ mrad the isotropic Ni surface is larger than that of Ni_3Al.

Despite the differences between the isotropic curves, a similar overall structure is found for Ni and Ni_3Al in the anisotropic curves. The individual peaks appear, however, to be different.

The difference curves in Fig. 6 illustrate some details of the surface. For Ni_3Al two peaks are seen symmetrically around 4.79 mrad, which fold into one another in k-space (Fig. 6(e)). Figure 6(d) is a section through the data from the (R,M) point along the $[1\bar{1}0]$ direction. The peak near 0 mrad also folds back into the two peaks shown in Fig. 6(e). These details are most likely originating from the R_{18}/R_{19} parts of the Fermi surface, and the multiple manifestation of the same structure in several zones is often called "Umklapp". By reading the peaks of Fig. 6(f) for Ni_3Al to the nearest integer channel in p-space and calculating the corresponding position in k-space, one obtains Fig. 7 showing k-space versus p-space position in the [100] direction. Figure 7 demonstrates that the peaks in p-space are highly ordered in k-space for Ni_3Al and a similar result may be obtained for Ni. From Fig. 6 and 7 it is seen that structures are contributing significantly in k-space up to $p \approx 15$ mrad and therefore any systematic errors in either the dispersion relationship (mrad/channel), linearities, or lattice constants could cause a loss of resolution or displacement of features in k-space. It is pointed out that coincidence of such peaks cannot be caused by the C_{4v} symmetrization of the data, since none of the symmetry elements in this group would carry any of these peaks into another.

From Figs. 6 and 7 two important conclusions can be made. Firstly, it is demonstrated that "Umklapps" are observed up to ≈15 mrad, and secondly that the anisotropic spectrum has a significant contribution from rapidly varying structures normally associated with the Fermi surface topology. All details observed in Fig. 6 need not originate from the Fermi surface however; the experiment can only

distinguish between details due to the Fermi surface and others to within experimental resolution.

A k-space representation of the isotropic Ni_3Ni and Ni_3Al surfaces are shown in Fig. 8. The surfaces are smooth and isotropic in p-space, but are structured and anisotropic in k-space. For Ni_3Al, a flat region near the X point is seen, and a bump in the surface is found along the Γ-M direction. Since this surface contains the major part of the observed events, one may suggest that it is dominated by the filled-electron bands and that such bands, in agreement with the calculations for Ni_3Ga (Shiotani et al. 1986, Kubo and Wakoh 1987), contribute significantly to the anisotropy in k-space. As a simple measure of the degree of anisotropy in k-space, one may take the relative variation from the (Γ,X) point to the (R,M) point; this variation is 13%.

The k-space representation of the isotropic Ni_3Ni data are also shown in Fig 8. The degree of anisotropy for this surface is ≈10%, approximately the same as that for Ni_3Al, and the surfaces look similar. Some differences are found however; the bump found in Ni_3Al is not seen in Ni_3Ni and the flat area near the X point is missing. The similarities between Ni_3Ni and Ni_3Al suggest that a major fraction of the anisotropy found in Ni_3Al can be understood in terms of folding the bands in Ni back into the smaller zone. The structures found in the isotropic surface for Ni_3Al and not for Ni_3Ni are, however, likely to be a consequence of differences between the bands in Ni_3Ni and Ni_3Al.

The k-space representations of the anisotropic data are shown in Fig. 9. It should be noted that the Ni_3Ni data have been obtained using 0.34 mrad/channel, resulting in less apparent structure.

Some of the major features are common to Ni_3Ni and Ni_3Al. The anisotropies are similar; a flat region from about 2.2 to 2.5 mrad running parallel to the [100]

directions is found in both figures and a pronounced k-dependence, including contributions from the Fermi surface, in the region of the (R,M) point is also seen in both. Features found along the Γ-M axis are much alike except for the region around the Γ point. Thus the anisotropic data for Ni_3Ni and Ni_3Al are similar.

The similarities of Ni_3Al and Ni_3Ni as observed from Figs. 8 and 9 strongly suggest that a comparison of theoretical calculations of the band structure for Ni_3Ga, Ni_3Al and Ni_3Ni would be an important contribution to the understanding of the electronic structure of these materials.

The calculations of Buiting et al. (1983) and the Ni_3Al data are compared in Fig.10. Some of the Fermi surface intersections with the high symmetry planes have been projected onto the (001) plane. Strictly, one should have projected the Fermi surface at points where it is tangential to [001], making the present plot an approximation.

The agreement between the calculations and experimental results is good, although systematic deviations, some of which are due to the experimental limitations, may be found. For example, the strong protuberance near 2.1 mrad on the [100] direction could be due to a discrete channel effect, while structures such as those found above and below the [100] direction at 3 mrad are not likely to be related to the Fermi surface, but cannot be separated from the Fermi surface by the experiment due to the finite resolution. One may also note that the finite resolution could, at least in principle, result in some displacement of the apparent Fermi surface features if the k-space dependence of the filled bands is strong. Such a dependence has been reduced considerably in the present work by the subtraction of the isotropic p-space dependence. In addition, a structure seen on the [110] direction (projecting at ≈1.5 mrad onto the [100] direction) is found in both Ni_3Al and Ni_3Ni. The origin of this feature is not understood, and will, for the present, be

assumed to be unrelated to the Fermi surface.

The contour plot is expected to be complicated in regions where the integration direction crosses the Fermi surface repeatedly, and can only be interpreted in simple terms near the high-symmetry directions. This is not a limitation to the 2-D ACAR technique since it can be alleviated by a reconstruction from multiple projections.

The details of Fig.10 will now be discussed. The Γ_{14}/Γ_{15} surfaces cannot be individually resolved, but parts of them may possibly be seen along the Γ-M direction in good agreement with theory. Since these surfaces are close to the Γ point, they are expected to be less visible in the Γ-X direction, due to positron-annihilation selection rules (Harthoorn and Minjarends 1978, Minjarends 1983). The projection of the neck around the X point above Γ (Γ_{17} sheet) is seen in agreement with theory to within experimental error. The nearby parts (in Γ-X direction) of the Γ_{16} sheet are poorly resolved from Γ_{17} . The corner of Γ_{17} in the (001) plane on the Γ-M axis possibly observed by the experiment appears slightly closer to the Γ point than theoretically predicted. In the Γ-M direction the protrusion of Γ_{16} in the (001) plane and the projection of the Γ_{17} lobe in the [111] direction onto the (001) plane are seen, but cannot be resolved from one another experimentally. In addition, the Γ_{16} protrusion should also be seen projected onto the Γ-X axis. The data are consistent in this regard; the structure on the Γ-M axis is directly above a corresponding structure along Γ-X. It can, therefore, be argued that the protrusion of the Γ_{16} sheet in the (001) plane along the [110] direction has been seen, while it is less certain that the Γ_{17} lobe along [111] has been observed. The projection of the Γ_{16} lobe in the [111] direction onto the (001) plane is also seen, while the R_{18}/R_{19} sheets are not, possibly because the contours in Fig. 10 do not span the entire zone.

From Fig. 10 one concludes that there is good agreement between the present data and the calculations of Buiting et al. (1983), although some systematic deviations are found. It is not clear at present whether they are real, or if they are due to the limitations of the experiment.

Conclusion:

It has been shown that Ni_3Al has a strong anisotropy in k-space, most likely due to the filled bands. However, a similar anisotropy was found for Ni_3Ni as well and it was suggested that a large fraction of the anisotropy could be understood in terms of folding the electron bands in Ni back into the first zone of Ni_3Ni.

The present work focussed mainly on the Fermi surface topology, but it should be noted that the 2-D ACAR data provide substantial information about the filled bands, which is not provided by most other techniques (e.g. dHvA). It would be interesting to pursue further the differences among the filled bands for the Ni_3Ni, Ni_3Ga, and Ni_3Al alloys; this will also require additional theoretical studies.

In regard to Fermi surface topology studies, it was demonstrated that the k-space dependence could be significantly reduced by the subtraction of an isotropic p-space dependence, and that in so doing, "Umklapp's" could be observed in both Ni and Ni_3Al up to $p \approx 15$ mrad.

When the remaining anisotropic k-space dependence for Ni_3Ni and Ni_3Al were compared, it was found that the structures were similar overall, while differences, most likely due to the Fermi surface topology, were seen in certain details of the structure.

The data for Ni_3Al were compared with theoretical Fermi surface calculations and a general agreement was found. More importantly, the Γ_{16} surface, predicted by theory, but so far not observed in any experiment, has been verified

here for the first time.

Acknowledgements:

The authors would like to thank R. W. Siegel for valuable guidance and encouragement. Helpful discussions with R. Benedek are gratefully acknowledged. We would also like to thank A. Dhere, W. H. Farmer, and E. H. Lee for help rendered at various stages of sample characterization and heat treatment. We are grateful to United Technologies for supplying the directionally solidified Ni_3Al samples, used as the starting material.

Figure captions:

Fig. 1. Optical microstructure of the directionally solidified $Ni_{76.5}Al_{23.5}$ alloy before heat treatment. The whole casting consists of a single dendrite of the γ' phase (ordered $L1_2$ structure), grown parallel to the [100] direction, which is seen as the light matrix phase in the microstructure. A fine network of the γ phase is seen around the γ' regions inside the dendrite arms.

Fig. 2. Three-dimensional representation of the 2-D ACAR surface in Ni_3Al. All data have been folded back into the first Brillouin zone.

Fig. 3. Contour plot of 2-D ACAR surface in Ni_3Al. All data have been folded back into the first Brillouin zone. There are $\approx 1.9\times10^6$ counts/mrad^2 in the center (Γ,X), the variation from the (Γ,X) point to the (R,M) point is $\approx 3.7\times10^5$ counts/mrad^2 and 70 equidistant contours are plotted. The zone boundaries are also shown.

Fig. 4. Calculated Fermi surface for Ni_3Al (Buiting et al. 1983). Intersections between the surface and high symmetry planes are shown.

Fig. 5. Comparison of anisotropy for Ni_3Al in the [110]-[100] directions for 1-D ACAR data (upper) and 2-D ACAR data (lower). The standard deviation at zero mrad for the 2-D ACAR data is indicated; the standard deviation is smaller at larger momenta.

Fig. 6. Sections through the 2-D ACAR surfaces for Ni and Ni_3Al.
Left frame: Ni, right frame: Ni_3Al.
Upper part: Sections through the 2-D ACAR surface a) [110], b) [100], c) isotropic.
Lower part: Sections through the 2-D ACAR surface after subtraction of isotropic curve. Sections: d) $[1\bar{1}0]$ starting at (R,M) in first zone of

Ni_3Ni and Ni_3Al, e) [110], f) [100]. Relative scales are indicated and standard deviations at 0 and 11 mrad are shown at curve f for Ni_3Al.

Fig. 7. Comparison of structures in p- and k-space along [100] for Ni_3Al. The peaks shown in Fig. 6 (e) are read off to the nearest integer channel and the k-space location is plotted versus p-space location. Lines are drawn through points with common k-space position.

Fig. 8. Isotropic 2-D ACAR surfaces for Ni_3Ni and Ni_3Al in k-space representation.

Left frame: Ni_3Ni. The surface is lowest at the (Γ,X) point having $2.9 \cdot 10^6$ counts/mrad^2. A range of $3.0 \cdot 10^5$ counts/mrad^2 is plotted using 70 equidistant contours to the highest point at (R,M).

Right frame: Ni_3Al. The surface is lowest at the (Γ,X) point having 1.9×10^6 counts/mrad^2. A range of 2.5×10^5 counts/mrad^2 is plotted using 70 equidistant contours to the highest point at (R,M).

Fig. 9. Anisotropic 2-D ACAR surface for Ni_3Ni and Ni_3Al in k-space representation.

Left frame: Ni_3Ni. The surface is lowest at the (Γ,X) point ($7.5 \cdot 10^4$ counts/mrad^2) and highest at the (R,M) point (1.9×10^5 counts/mrad^2). 70 contours are plotted.

Right frame: Ni_3Al. The surface is lowest at the (Γ,X) point (0 counts/mrad^2) and highest at the (R,M) point (1.3×10^5 counts/mrad^2). 70 contours are plotted.

Fig. 10. Anisotropic 2-D ACAR surface for Ni_3Al in k-space representation with the Fermi surface calculated by Buiting et al. (1983) overlaid. Bold curves are intersections of the Fermi surface and the (001) plane, while light curves are projections from other high symmetry planes.

Starting at Γ and going towards X: (Γ_{14}/Γ_{15}), the Γ_{17} neck projected from the MXR plane, Γ_{16} coinciding with Γ_{16} projected from the ΓXR plane, and Γ_{16} projected from the ΓMR plane. Starting at Γ and going towards M: (Γ_{14}/Γ_{15}), the Γ_{17} neck projected from the MXR plane, Γ_{17}, Γ_{16}, Γ_{17} projected from the ΓXR plane, Γ_{16} projected from the ΓXR plane coinciding with Γ_{16} projected from the ΓMR plane, and R_{18}/R_{19} projected from the MXR plane.

References:

Berko S., Haghgooie, M. and Mader, J.J., Phys. Letters A 63, 335 (1977)

Berko S. in "Proceedings of the International School of Physics, Enrico Fermi," eds. W. Brandt and A. Dupasquier, North Holland (1983), p. 64.

Buiting J. J. M., Kübler J., and Mueller F. M., J. Phys. F: Met. Phys., 13, L179 (1983).

Bull C. R. , West R. N., Kawamiya N., and Shiotani N. in "Positron Annihilation", eds. P. C. Jain, R. M. Singru, and K. P. Gopinathan, World Scientific Publishing Co., Singapore (1985), p. 40.

Fletcher G. C., Physica, 56, 173 (1971), Physica, 62, 41 (1972)

Gell M. , Duhl D. N., and Giamei A. F., Superalloys 1980, Proc. of the Fourth Intern. Symp. on Superalloys, J. K. Tien, S. T. Wlodek, H. Morrow III, M. Gell, and G. E. Maurer (eds.), ASM, Metals Park (1980), pp. 205-214.

Harthoorn R. and Minjarends P. E., J. Phys. F: Met Phys., 8, 1147 (1978).

Kubo Y. and Wakoh S. , Sci. Rep. Univ. Library Infor. Sci., 2 , 11, (1983), J. Phys. F: Met Phys., 17 397 (1987).

Lock D. G., Crisp V. H. C., and West R. N., J. Phys. F: Met Phys., 3, 561 (1973).

Minjarends P. E. in "Proceedings of the International School of Physics, Enrico Fermi," eds. W. Brandt and A. Dupasquier, North Holland (1983), p. 146.

Moriya, T., J. Magn. Magn. Mat., 14, 1 (1979)

Shoitani N., Bull C. R., West R. N., Kawamiya N., Kubo Y., and Wakoh S., J. Phys. Soc. Japan 55, 1961 (1986).

Sigfusson T. I. , Bernhoeft N. R., and Lonzarich G. G. , J. Phys. F: Met. Phys., 14, 2141 (1984).

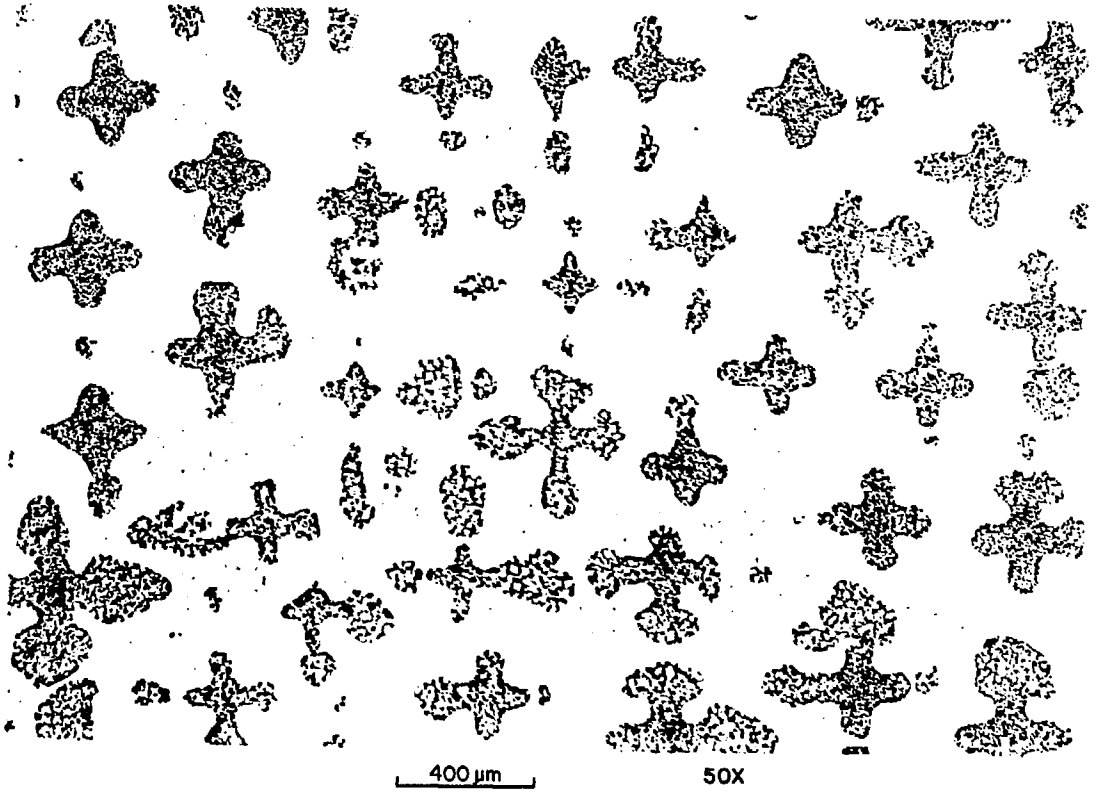
400 µm
50X

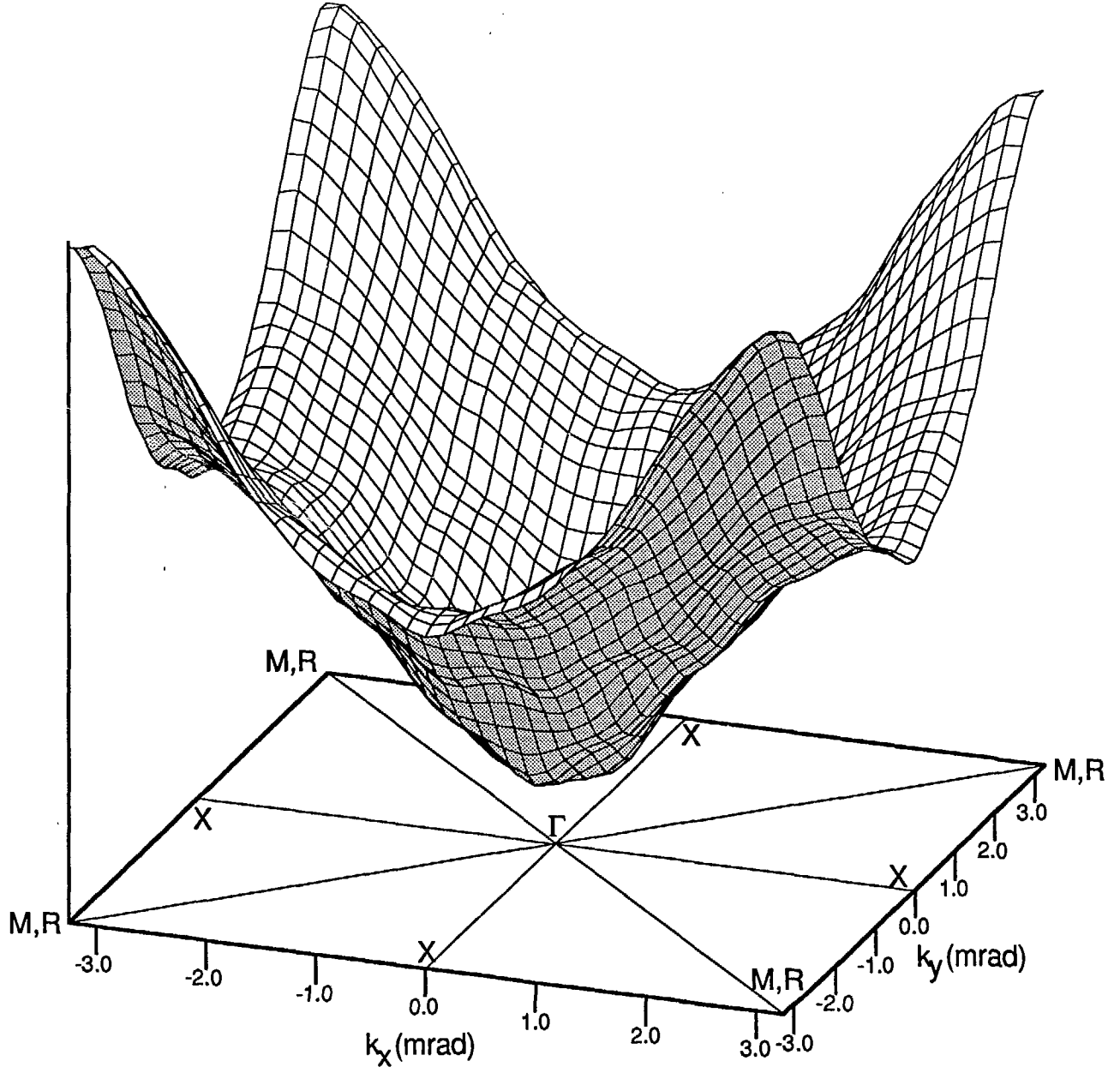
M,R
X
M,R
X
Γ
X
M,R
M,R
X
M,R
-3.0
-2.0
-1.0
0.0
1.0
2.0
3.0
k_x(mrad)
-3.0
-2.0
-1.0
0.0
1.0
2.0
3.0
k_y(mrad)

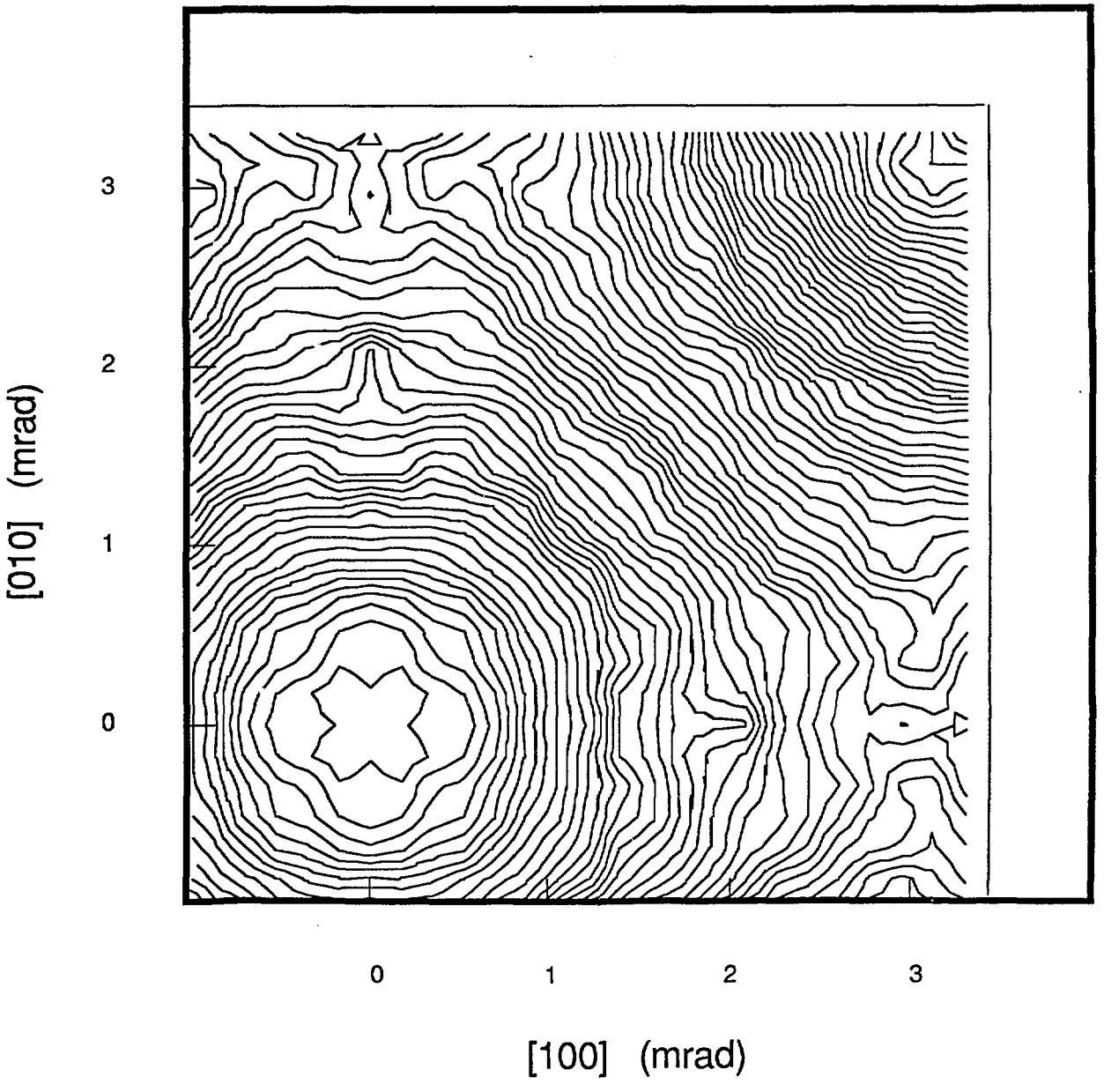
3
2
1
0
[010] (mrad)
0
1
2
3
[100] (mrad)

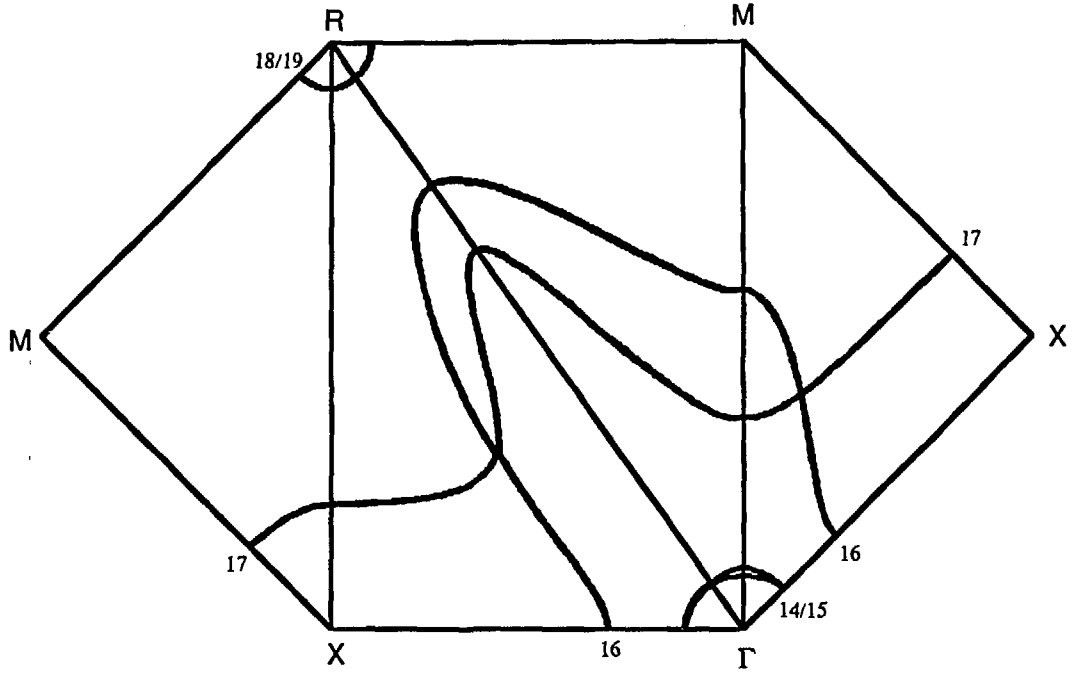
R
M
18/19
17
M
X
17
16
14/15
X
16
Γ

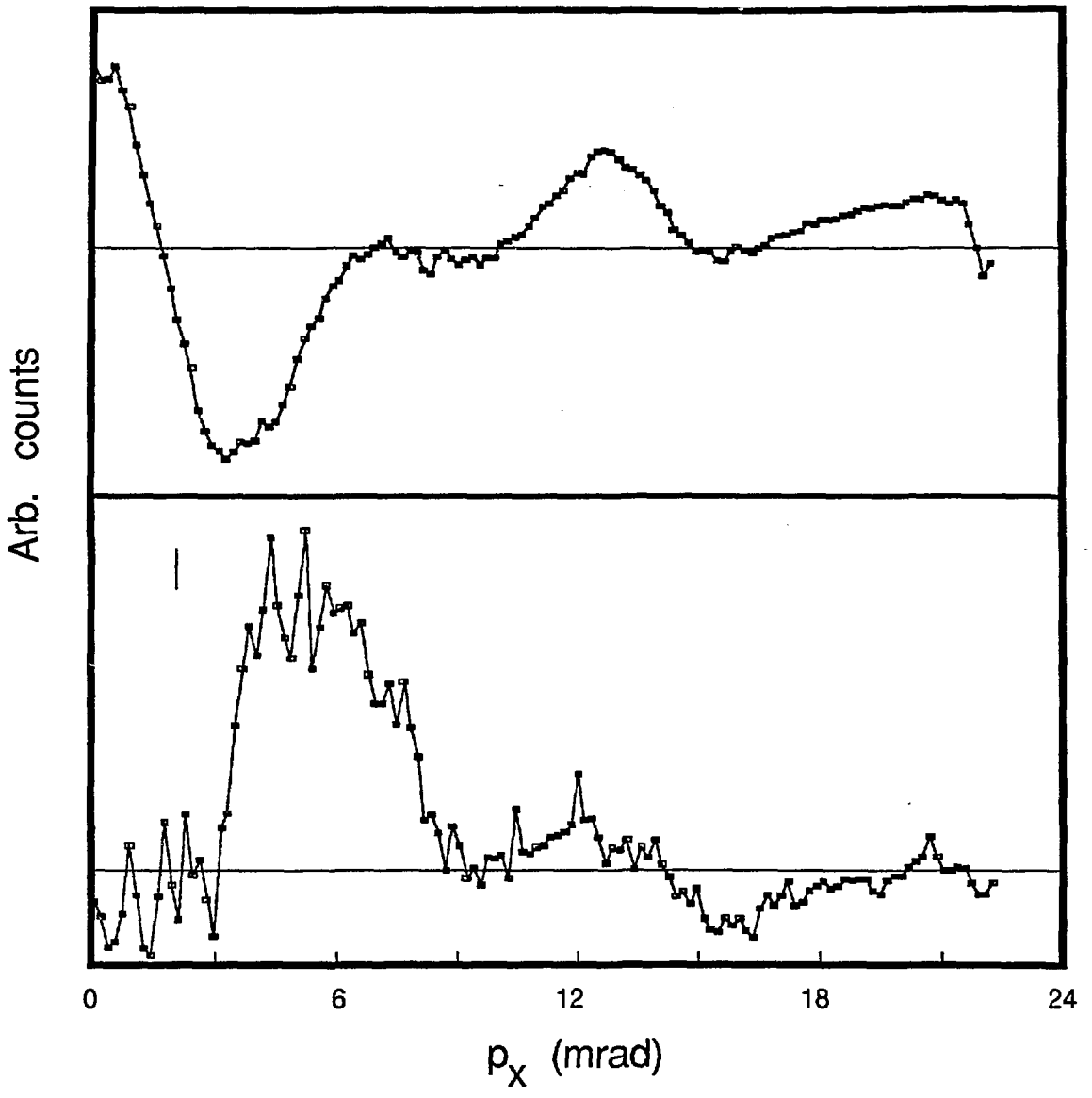
Arb. counts
0
6
12
18
24
p_x (mrad)

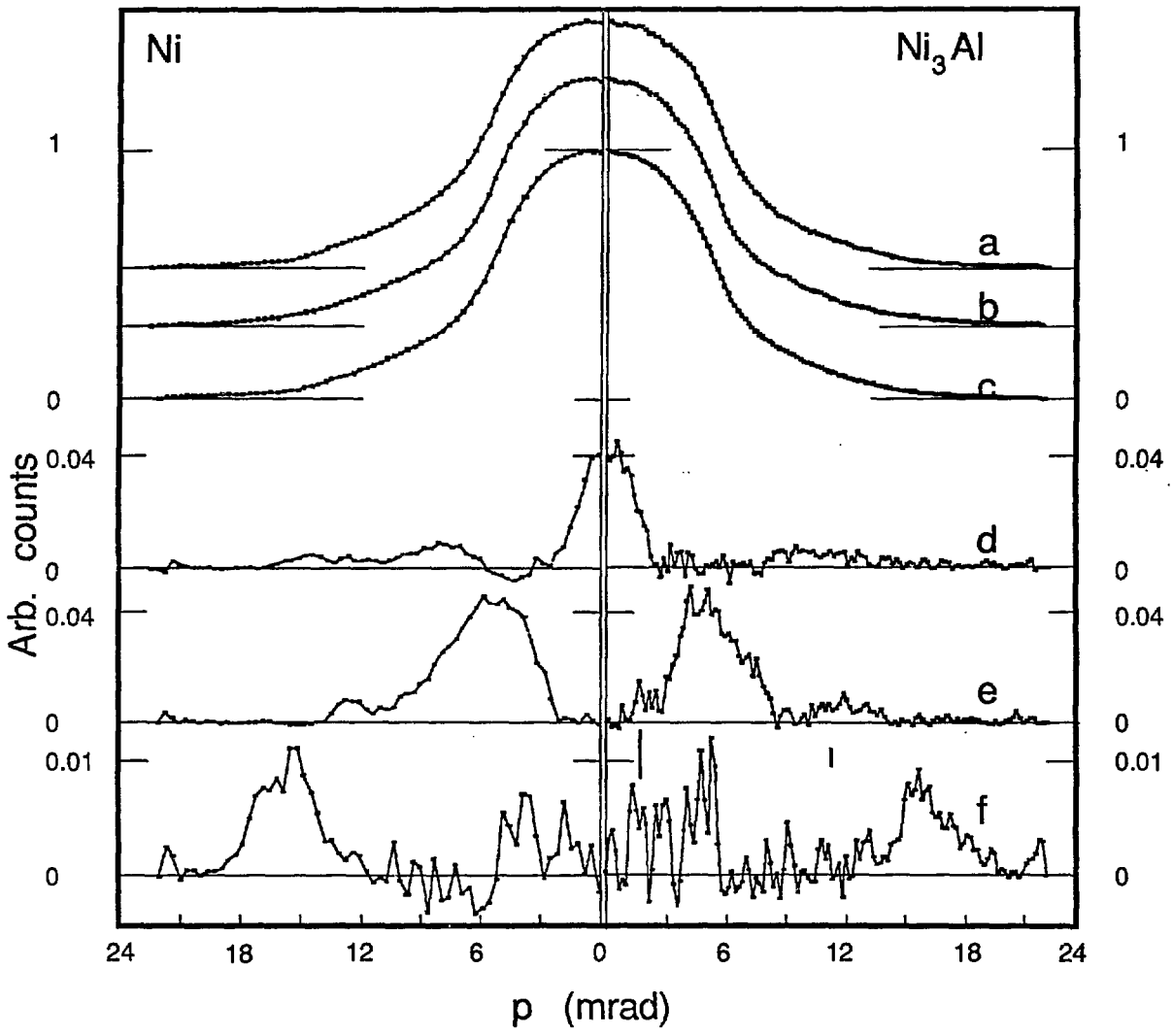
Ni
Ni3Al
a
b
c
d
e
f
1
0
0.04
0.01
Arb. counts
24
18
12
6
0
p (mrad)

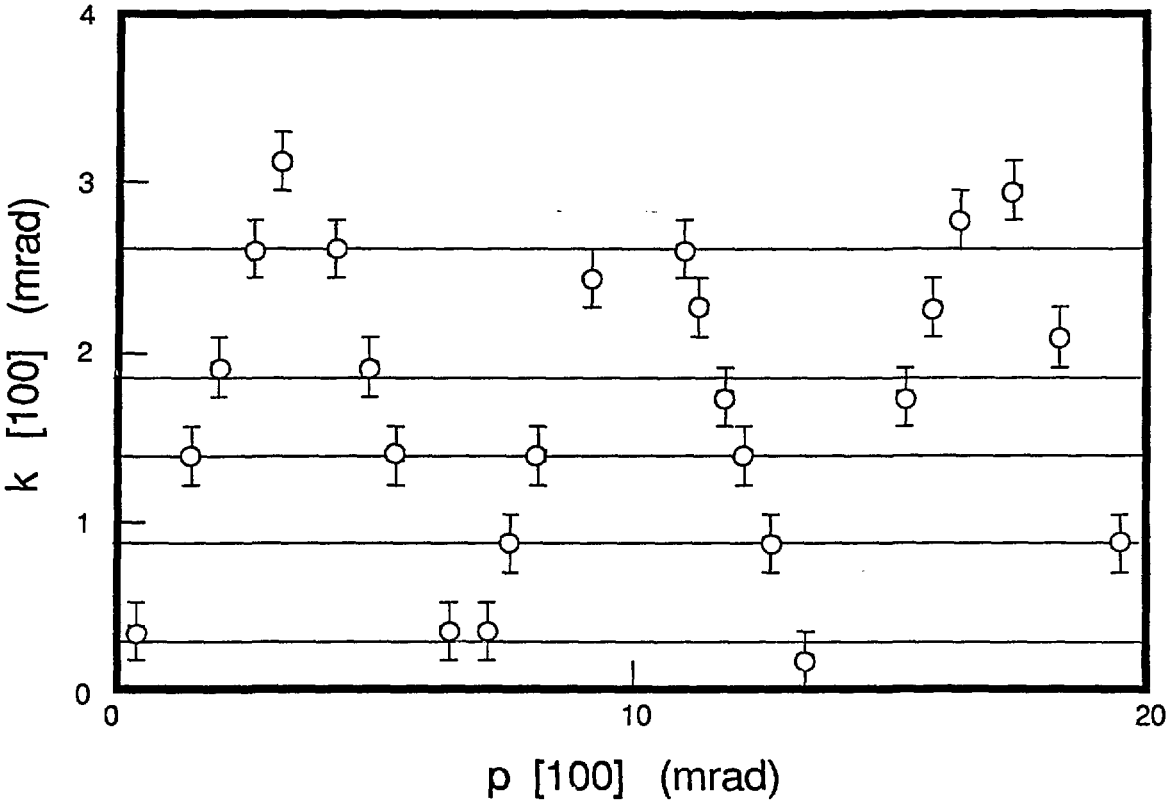
4
3
2
1
0
k [100] (mrad)
0
10
20
p [100] (mrad)

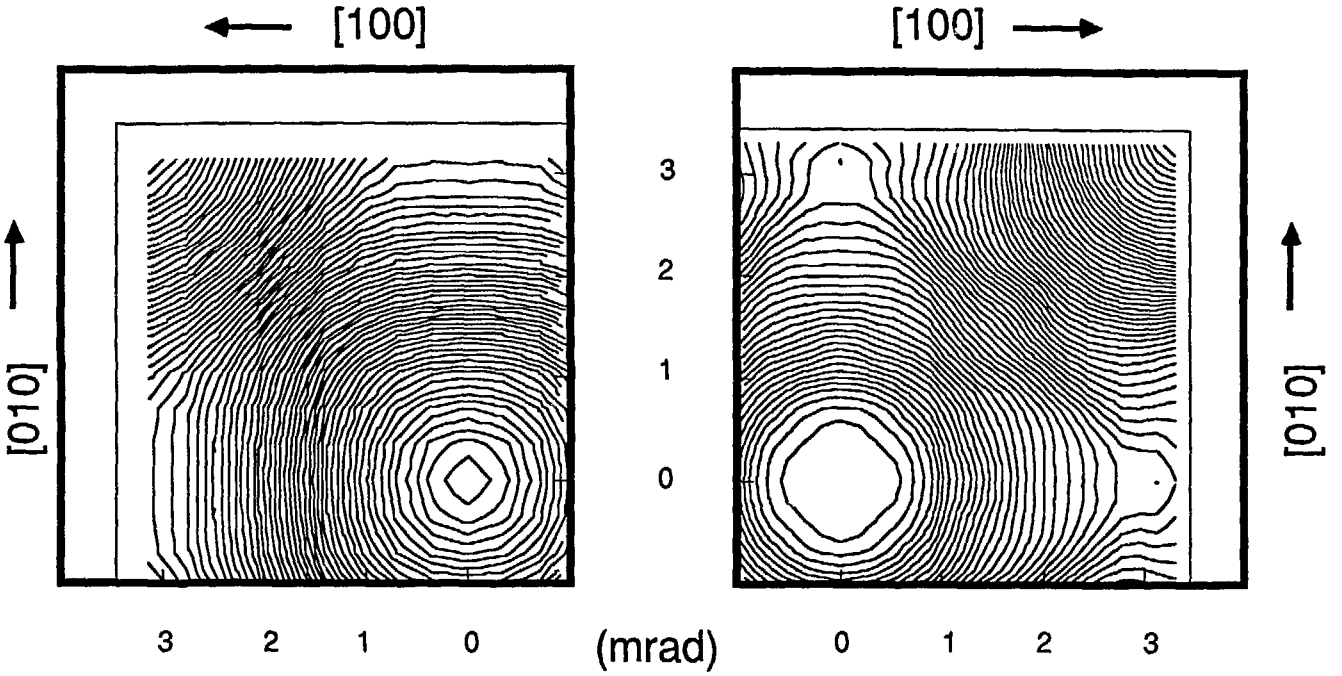
[100]
[100]
[010]
[010]
3
2
1
0
3 2 1 0
(mrad)
0 1 2 3

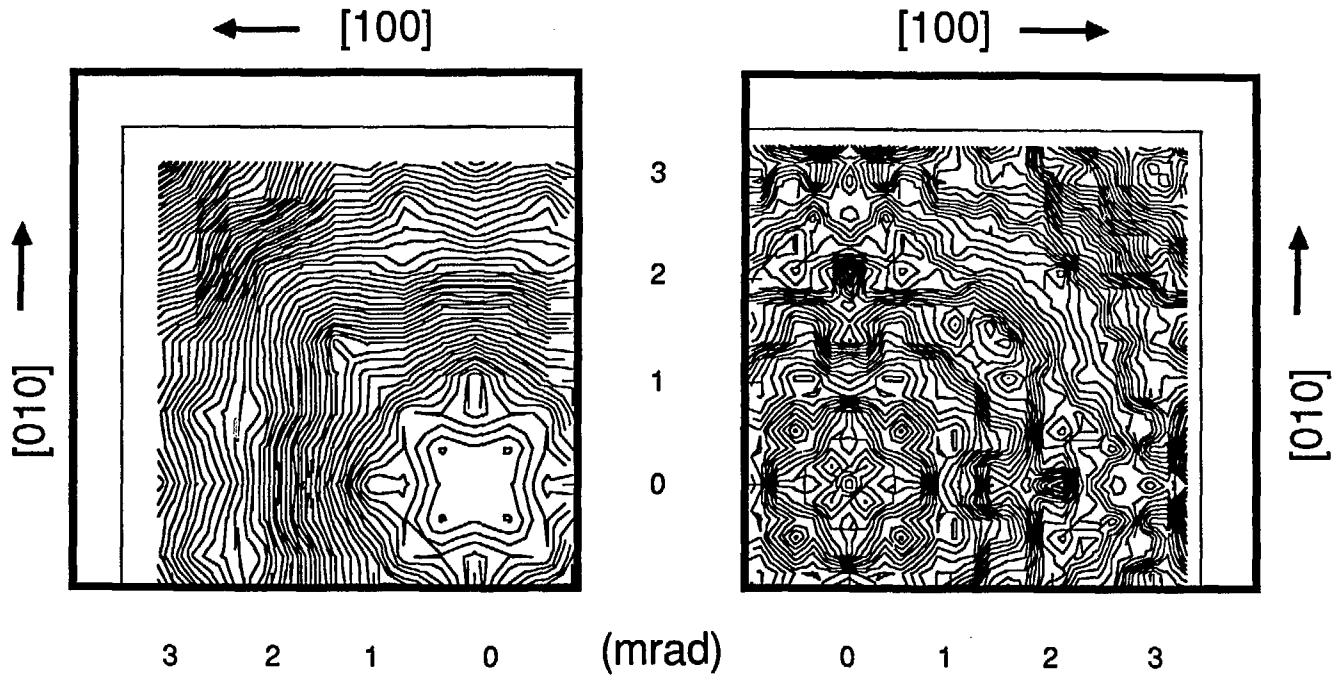

Fig 9

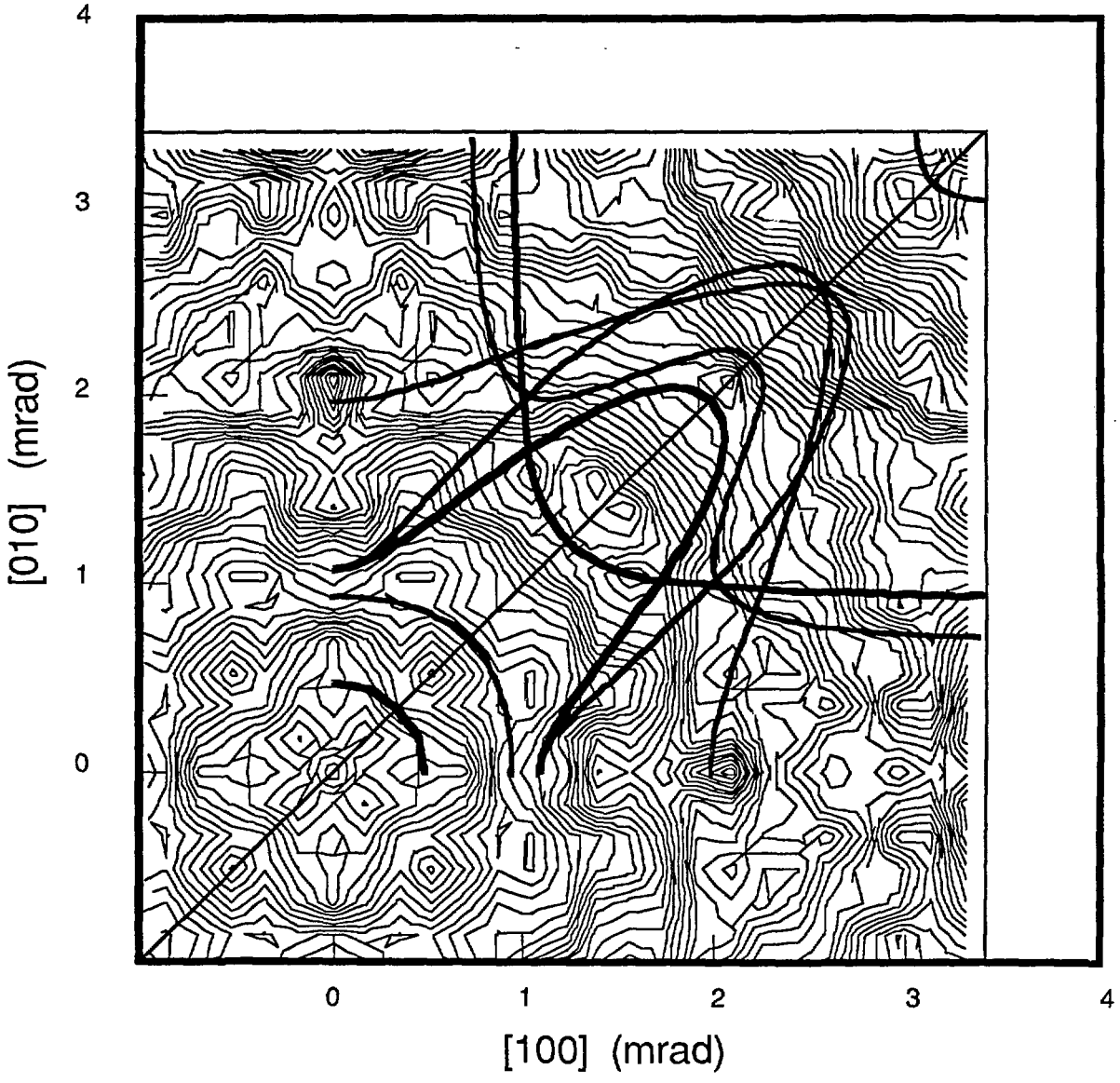
4
3
2
1
0
[010] (mrad)
0
1
2
3
4
[100] (mrad)